Large Mode Area Pr^{3+}- doped Chalcogenide PCF Design for High Efficiency Mid-IR Laser

M A Khamis, R Sevilla and K Ennser

Abstract*— We propose a novel design of a photonic crystal fiber made of praseodymium (Pr^{3+})-doped chalcogenide glass with single mode operation beyond 4 μm. Our design has an enlarged Pr^{3+}-doped core diameter of 60 μm. The field area of the emitted fundamental mode is about 3160 μm^2 at 4.5 μm and 2050 μm^2 at a pump wavelength of 2.04 μm. This large mode field area not only reduces the nonlinear effects but also increases the possible pump power before the damage threshold. The selected laser layout avoids fabrication difficulties associated to cascaded Fiber Bragg Gratings in Pr^{3+}-doped chalcogenide glass fibers. The proposed design also increases the laser efficiency by using the overlap of the emission cross-sections of Pr^{3+} in the transitions ($^3F_2$, $^3H_6 \rightarrow {}^3H_5$ and $^3H_5 \rightarrow {}^3H_4$) to enable both transitions to simultaneously produce a single coherent mid-infrared wavelength. The simulation results reveal that more than 64% of slope efficiency could be achieved at 4.5 μm for a fiber loss of 1dB/m.

***Index Terms*— Mid-infrared fiber laser, Praseodymium doped-glass, Chalcogenide glass material, Photonic crystal fiber.**

I. Introduction

CONSIDERABLE effort has been recently devoted to the study of mid-infrared (Mid-IR) light sources due to the numerous applications in medicine and environmental monitoring [1-3]. Chalcogenide glasses allow one of the broadest Mid-IR transmission windows beyond 12μm. Chalcogenide materials have high refractive index, low losses, low phonon energy, good rare earth ion solubility and therefore it is attractive host material for rare earth ions [4-7]. Mid-IR lasers and amplifiers can be constructed from suitable rare earth ions doped with chalcogenide host material. Recently, it has been shown that Pr^{3+}-doped chalcogenide glass has attractive characteristics in the Mid-IR fluorescence due to their high pump absorption cross-section. In addition, Pr^{3+} can be pumped from a commercially available 2-μm diode laser. Furthermore, Pr^{3+}-ions have overlapping emission cross-sections in the ($^3F_2$, $^3H_6$) → $^3H_5$ (3.3–4.7 μm), and $^3H_5 \rightarrow {}^3H_4$ (3.7–5.5 μm) transitions [8,9]. However, laser levels ($^3F_2$, $^3H_6$) and $^3H_5$ have lifetimes of the same order, which makes difficult to create the population inversion. A cascade lasing approach is a possible solution to this latter obstacle but it produced low laser efficiency at 16% [9] and at 30% with a larger core diameter and high Pr^{3+} concentration [10]. In contrast, 48% efficiency is achieved by exploiting the overlapping emission cross-sections of Pr^{3+}-doped chalcogenide glass [8] and 54% efficiency has been reported using a resonantly pumped scheme [11].

Chalcogenide materials have high optical nonlinearity that has been successfully used for nonlinear-optical conversion of radiation in the Mid-IR [6]. The high-power density due to the confinement of light in the core (especially due to small core area) makes a fiber based laser system susceptible to nonlinear effects that ultimately limits the performance of fiber lasers and amplifiers [12]. Another problem on the design of Mid-IR chalcogenide fiber laser is related to a relatively low damage threshold [11].

To overcome these limitations, a large mode field area of the core is required to restrict the nonlinear effects and increase the possible pump power before the damage threshold. Unfortunately, the increasing of core diameter in a conventional fiber leads a transition to multimode guidance, which will cause the degradation of beam quality.

Photonic crystal fibers (PCFs) are a promising way to overcome the above difficulties. These fibers offer many optical characteristics including endlessly single-mode guidance, controllable chromatic dispersion, high birefringence, large mode area, and low bending losses [13]. Furthermore, PCF offers more design flexibility than a conventional fiber because it allows a fine control of the refractive index profile of both the core and the cladding.

In this letter, a Pr^{3+}-doped selenide glass PCF laser pumped at the wavelength of 2.04 μm is designed for enhancing the efficiency of Mid-IR light sources. A single pair of fiber Bragg gratings is used with Bragg wavelength in the range of the overlapping emission cross-sections (3.7–4.7 μm). Our proposed design has an intrinsically single-transverse-mode core with a diameter of 60 μm. The effective mode field area is about 3160 μm^2. Our results show that more than 64% of power efficiency could be theoretically achieved at wavelength of 4.5μm and fiber loss of 1dB/m.

II. Theory and Design

The proposed fiber cross-section is depicted in Fig. 1. The cladding with 200-μm diameter consists of a regular hole structure (diameter d and pitch Λ) in chalcogenide host (GeAsGaSe). The rare earth-doped solid core with d=60μm is formed by 19-missing holes surrounded by three rings of air holes. There are two limiting conditions in the design of PCF laser. The first condition is to ensure single mode guidance by

Submitted on February 14, 2018. This work was supported by the High Committee for Education Development in Iraq (HCED).

M. A. Khamis, R. Sevilla and K. Ennser are with College of Engineering, Swansea University, Bay Campus, Fabian Way, Swansea, SA1 8EN, Wales, United Kingdom. M. A. Khamis is also with Baqubah Technical Institute, Middle Technical University, Baghdad, Iraq.
(email:805172@swansea.ac.uk).

calculating the normalized frequency (V) of the doped core [14]:

$$V = \frac{2\pi a}{\lambda} \times NA = \frac{2\pi a}{\lambda}\sqrt{(n_{ch} + \Delta n)^2 - n_{cl}^2} \quad (1)$$

Where a is the core radius, λ is the laser wavelength, Δn is the refractive index increase caused by the rare-earth dopant within the core, n_{ch} is the chalcogenide refractive index (not rare earth doped) and n_{cl} is the effective refractive index of the cladding region.

The second condition is that the guidance must be dominated by the PCF cladding and not by the raised index (caused by co-dopants) [14]:

$$\Delta n < \left(\frac{n_{ch}^2 - n_{cl}^2}{2n_{ch}}\right) \quad (2)$$

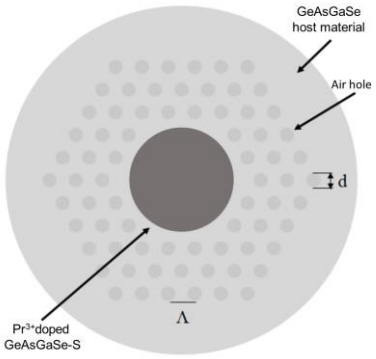

Fig. 1 Cross- section of photonic fiber, having 60-μm core diameter and 200-μm cladding diameter.

Figure 2 shows the variation of refractive index with wavelength for GeAsGaSe and Pr^{3+}:GeAsGaSe glass material [15]. Despite the effect of Pr^{3+}-doping in the step-index fiber is marginal, it must be considered in our PCF design to achieve the second condition of guidance properties.

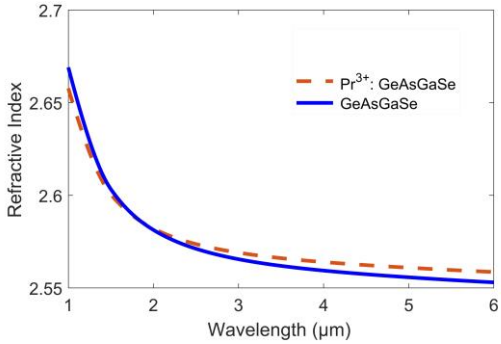

Fig. 2. The refractive index versus the wavelength for GeAsGaSe and Pr^{3+}: GeAsGaSe glass material.

To optimize the PCF design, we fix the pitch size (Λ) to 15 μm and optimize the hole diameter size to ensure the condition of a single-transverse-mode. The cladding effective index can be calculated by investigating the propagation of the fundamental space-filling mode of the perfect cladding structure [16]. Finite element method (FEM) based edge element analysis is used to calculate the cladding effective index. This approach based on vector basis functions eliminates the disadvantages of the scalar FEM approach of having undesired non-physical solutions and easy implementation of boundary conditions at material interfaces [17]. A Matlab program is built to do this task.

Figure 3 shows the optimum parameters for the doped PCF at 4-μm wavelength (the beginning of laser transition [8]). To solve eq. (1) and (2), we set V = 2.405. The dashed and solid lines in Fig. 3 indicate the value of Δn with respect to d/Λ from eq. (1) and (2), respectively at above assumption. Any structure located under the dashed line correspond to single-mode at the cut-off wavelength. The intersection point (vertical dashed line) between these two lines represents the solution of Δn at our approximation. So, the value of Δn must be close to this value. We choose $\Delta n = 2.7\times10^{-4}$ where $d/\Lambda = 0.53$ and the hole diameter equals 8 μm at Λ=15 μm. It is observed that the calculated Δn is less than the refractive index increase caused by the rare-earth dopant within the core. In this case, we substitute suitable percentage of Selenium (Se) by Sulphur (S) in the core region to lower the refractive index [18]. In our design, 0.8 at.% (atomic %) of S is enough to obtain the above Δn value.

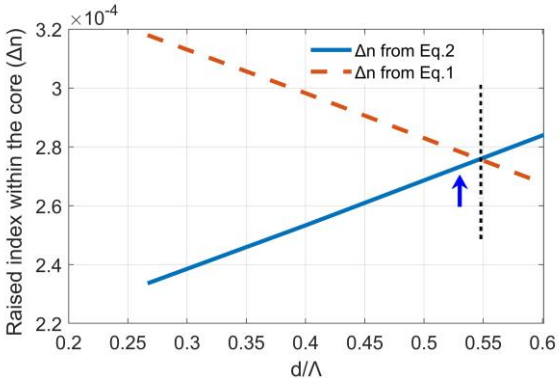

Fig. 3. Optimum parameter regime for doped PCF (Λ=15μm, λ=4μm). The doped core does not significantly influence the guidance for structures located under the solid line (Eq.2) and structures under the dashed line are SM (Eq.1).

After optimization of the fiber geometry, we can now calculate the confinement factors between the Pr^{3+}- doped area and the energy transverse distributions of the pump (Γ_p) and of the signal (Γ_s) as [12]:

$$\Gamma_z = \frac{\iint_0^r |E_z^2(x,y)|dxdy}{\iint_0^\infty |E_z^2(x,y)|dxdy} \quad (3)$$

Where z is either p for pump or s for signal, r is the radius of Pr^{3+}-doped area and $E_z^2(x,y)$ is the electric field intensity of the guided wave at the pump wavelength (λ_p) and the signal wavelength (λ_s). The effective mode field area can be expressed as:

$$A_{eff} = \frac{\left(\iint_{-\infty}^{\infty} |E_z(x,y)|^2 dxdy\right)^2}{\iint_{-\infty}^{\infty} |E_z(x,y)|^4 dxdy} \quad (4)$$

For the laser scheme, we use a single pair of FBG which its Bragg wavelength in the wavelength range of the overlapping emission cross-sections (3.7 μm-4.6 μm). They correspond to the emission cross-sections in the ($^3F_2$, $^3H_6$) → $^3H_5$ (3.3–4.7 μm), and $^3H_5 \rightarrow {}^3H_4$ (3.7–5.5 μm) transitions. We have previously demonstrated that this layout can achieve higher

laser efficiency without leading to fabrication difficulties caused by cascaded FBGs [8].

The employed model considers the pump absorption and stimulated emission close to the pump wavelength at 2.04 μm and the signal absorption and stimulated emission close to the signal wavelength at 4.5 μm. The laser steady state equations are taken from [8]. The spatial evolution of the pump and signal powers are obtained by solving the following differential equations:

$$\frac{dP_p^{\pm}}{dz} = \mp\Gamma_p\left[\sigma_{pa}N_1 - \sigma_{pe}N_3\right]P_p^{\pm} \mp \alpha P_p^{\pm} \quad (5)$$

$$\frac{dP_s^{\pm}}{dz} = \mp\Gamma_s[(\sigma_{ia}N_2 - \sigma_{ie}N_3) + (\sigma_{sa}N_1 - \sigma_{se}N_2)]P_s^{\pm} \mp \alpha P_s^{\pm} \quad (6)$$

Where Γ_p, Γ_s are the confinement factor for pump and signal, σ_{ij} is the absorption or emission cross-section for the ij transition, P_x denotes the propagating signal and pump powers, respectively, and α is the fiber loss. Note that the idler is the same to signal and under the overlapping transition wavelengths, therefore $P_i = P_s$, '+' and '-' refer to forward and backward travelling which are governed by the following boundary conditions:

$$P_s^{+}(0) = R_i\, P_s^{-}(0) \quad (7)$$

$$P_s^{-}(L) = R_o\, P_s^{+}(L) \quad (8)$$

Where R_i and R_o are the FBG reflectivity at the input and output of the Pr^{3+}-doped fiber, respectively; L is the laser cavity length. We numerically propagated the powers at λ_s back and forth between the mirrors, subject to the reflectivity at the fiber ends. The process is repeated iteratively until two adjacent iterations are close enough ($\leq 10^{-6}$).

III. Numerical results

First, we computed the electric field distribution of the fundamental mode versus wavelength of the fiber with our FEM software. Figure 4 illustrates the electric field norm distribution of the fundamental mode at the wavelength λs = 4.5μm. It can be clearly seen that the optical field is confined in the doped core region of the fiber.

The confinement factors and effective mode-field area versus the wavelengths are plotted in Fig. 5. We can clearly notice that large effective mode area can be achieved and they are increased linearly versus the wavelengths. In addition, the proposed fiber design produces a large confinement factor with very low dependence on the wavelength, contrary to conventional fibers [9]. This is because for a conventional fiber the difference between the core/clad refractive index remains constant as the wavelength increases, whereas for a PCF it increases. These larger confinement factors will enhance the laser performance as well as the optical efficiency.

The parameters used in the numerical simulations of the laser scheme are taken from [8] and are as follows: Pr^{3+}-ion concentration is 5×10^{25} ions/m^3, the lifetime of level 2 ($^3H_5$) and level 3 ($^3F_2$, $^3H_6$) equal to 12ms and 4.2ms, respectively. The branching ratio for 3-2 is 0.42. The resonator structure of the fiber laser consists of a pair of FBG to trap the signal. The reflectivity of the input FBG for the pump wavelength is 0.05 and for the signal is 0.95, while the output reflectivity is 0.05 for the signal [9].

Relaxation method is used to solve the differential equations (5) and (6) of the pump and the signal, respectively. We assume the level of losses for the pump and signal wavelengths are 1 dB/m and this value is much higher than the value used in experiments for some chalcogenide glass [9]. Using the values of the emission and the absorption cross-section spectra [9], we solve numerically the rate equations of the pump model. We investigate the important parameters such as the cavity length and pump power to evaluate their influence in the laser performance.

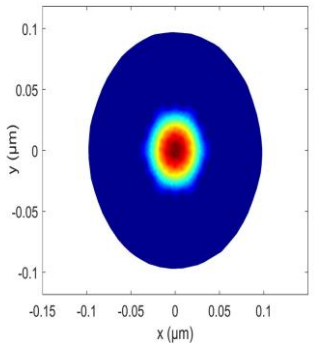

Fig. 4 The electric field norm distribution of the fundamental mode at the wavelength λs = 4.5μm.

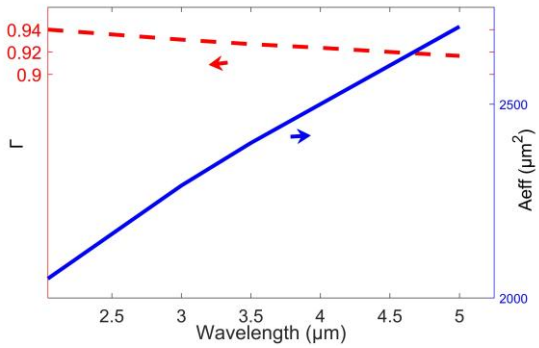

Fig. 5 The variation of confinement factors (dashed line) and mode field area (sold line) versus the wavelengths for the proposed PCF design.

We find a slope efficiency which is the slope curve obtained from plotting the output power with respect to input pump power. Figure 6a shows the slope efficiency versus laser cavity length L for different input pump powers. The results indicate that, for all pump power cases considered, the slope efficiency increases with the laser cavity length until a maximum is reached. After that, the slope efficiently drops due to the increase in fiber losses and the reduction in population inversions as a function of the cavity length. More than 64% of slope efficiency at λ_s=4.5μm can be achieved for the optical cavity length L= 0.45m and a pump power of 1W corresponding to a power intensity of 488MW/m^2.

Table I shows a comparison of the proposed design with previously reported results for the same fiber loss at 1dB/m. Our proposed fiber design exhibits the advantage of high laser efficiency with a lower applied pump intensity than previously reported Mid-IR chalcogenide fiber lasers.

Figure 6b shows the dependence of the laser efficiency with the fiber loss after considering the impurity loss such as Se-H

which is experimentally hard to remove [19]. Note that it is still possible to achieve lasing action with loss levels higher than 1dB/m for a pump at 2μm as the required PCF length is relatively short. As a result, our fiber design not only enhances the laser performance but also reduces the influence of the chalcogenide fiber loss

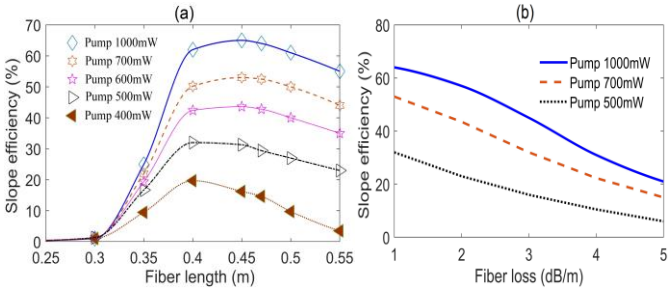

Fig. 6. a) Calculated output slope efficiency versus the laser cavity length with different pump powers. b) The dependence of the output slope efficiency on the fiber loss.

TABLE I
A COMPARISON OF OUR DESIGN WITH PREVIOUSLY REPORTED RESULTS

Laser layout	Area (μm^2)	Pump intensity (MW/m^2)	Slope efficiency
SIF with cascade lasing approach [9]	2827	1768	16%
SIF with overlapping approach [8]	2827	1768	48%
Multi-mode SIF with in resonantly pumped scheme [11]	707	1414	54%
PCF (current design)	2050	500	64%

IV. CONCLUSION

In this letter, we have proposed a Pr^{3+}-doped chalcogenide PCF laser operating at λ_s=4.5μm. A theoretical study to optimize a single mode Pr^{3+}-doped chalcogenide PCF is carried out. Our proposed design enlarges the Pr^{3+} doped core region to 60 μm by missing first 19 holes and wider the pitch size to Λ=15μm. The mode field area of the emitted fundamental mode is about 3160 μm^2 at 4.5μm and 2050μm^2 at a pump wavelength λ_p=2.04μm. This large effective mode field area can limit any impact of the nonlinearity and increases the damage threshold power. Moreover, the confinement factors exceed the value of 0.94 and 0.92 at the pump and the signal wavelengths, respectively. These larger confinement factors enhance the laser performance and increases the optical efficiency.

The laser layout avoids fabrication difficulties of cascaded FBGs in Pr^{3+}-doped chalcogenide glass fiber. We use the overlap of the emission cross-sections of Pr^{3+} in the transitions ($^3F_2$, $^3H_6 \rightarrow {}^3H_5$ and $^3H_5 \rightarrow {}^3H_4$) to enable both transitions to simultaneously produce a single coherent Mid-IR wavelength. Exploiting this characteristic, the proposed design uses only one pair of FBG for idler and signal. Hence, it avoids the fabrication complexity which is related to the construction of two pairs of Bragg gratings and two lasing cavities. In addition, one excited ion in this approach can emit two photons in Mid IR wavelengths as the same process in cross-relaxation transition of Tm^{3+}-doped fiber laser and therefore it increases the slope efficiency. The simulation results reveal that more than 64% of slope efficiency could be achieved at wavelength of 4.5μm and fiber loss of 1dB/m. To the best of our knowledge, this work produced the highest efficiency Pr^{3+}-doped chalcogenide glass fibers at 4.5 μm.

REFERENCES

[1] H. Jelínková et al., "Comparison of mid infrared lasers effect on ureter tissue," Laser Phys. Lett., vol.1, no.3, pp.143–146, 2004.
[2] F. Starecki et al., "Mid-IR optical sensor for CO2 detection based on fluorescence absorbance of Dy^{3+}: $Ga_5Ge_{20}Sb_{10}S_{65}$ fibers," Sens. Actuator B, Chem., vol. 207, no. 5, pp.518–525, Sep. 2015.
[3] M.L. Anne et al.," Fiber evanescent wave spectroscopy using the mid-infrared provides useful fingerprints for metabolic profiling in humans," J. Biomed. Opt., vol.14, no.5, pp.054033-054039, 2009.
[4] L. B. Shaw, B. Cole, P. A. Thielen, J. S. Sanghera, and I. D. Aggarwal, "Mid-wave IR and long-wave IR laser potential of rare-earth doped chalcogenide glass fiber," IEEE J. of Quantum Electron, vol.37, no.9, pp.1127–1137, 2001.
[5] R. G. DeCorby et al., "High-index-contrast waveguides in chalcogenide glass and polymer," IEEE J. Sel. Top. Quantum Electron, vol.11, no.2, pp.539-546, 2005.
[6] C R. Petersen et al., "Mid-infrared supercontinuum covering the 1.4–13.3 μm molecular fingerprint region using ultra-high NA chalcogenide step-index fibre" Nature Photonics, vol.8, pp.830–834, 2014.
[7] G. E. Snopatin, V. S. Shiryaev, V. G. Plotnichenko, E. M. Dianov, and M. F. Churbanov, "High-purity chalcogenide glasses for fiber optics," Inorg Mater, vol.45, no.13, pp.1439–1460, 2009.
[8] M. A. Khamis and K. Ennser, "Design of Highly Efficient Pr^{3+}-doped Chalcogenide Fiber Laser," IEEE Photon. Technol. Lett., vol.29, no.18, pp.1580–1583, Aug. 2017.
[9] Ł. Sójka, Z. Tang, H. Zhu, E. Bereś-Pawlik, D. Furniss, A. B. Seddon, T. M. Benson, and S. Sujecki, "Study of mid-infrared laser action in chalcogenide rare earth doped glass with Dy^{3+}, $Pr^{3+}$and Tb^{3+}," Opt. Mater. Express, vol.2, pp.1632-1640, 2012.
[10] E. V. Karaksina, V. S. Shiryaev, M. F. Churbanov, E. A. Anashkina, T. V. Kotereva, and G. E. Snopatin, "Core-clad Pr(3+)-doped Ga(In)-Ge-As-Se-(I) glass fibers: Preparation, investigation, simulation of laser characteristics," Opt. Mater., vol. 72, pp. 654–660, 2017.
[11] L. Sójka, Z. Tang, D. Furniss, H. Sakr, E. Bereś-Pawlik, A. B. Seddon, T. M. Benson, S. Sujecki, "Numerical and experimental investigation of mid-infrared laser action in resonantly pumped Pr^{3+} doped chalcogenide fibre," Opt. Quant. Electron., vol. 49, no. 21, 2017.
[12] S. Hilaire, D. Pagnoux, P. Roy, and S. Février, "Numerical study of single mode Er-doped microstructured fibers: influence of geometrical parameters on amplifier performances" Opt. Express, vol.14, pp. 10866-10877, 2006
[13] M. de Sario, L. Mescia, F. Prudenzano, F. Smektala, F. Deseveday, V. Nazabal, J. Troles, and L. Brilland, "Feasibility of Er^{3+}-doped, $Ga_5Ge_{20}Sb_{10}S_{65}$ chalcogenide microstructuresd optical fiber amplifiers", Opt. Laser Technology, vol.21, pp. 99-106, 2009.
[14] K. Hougaard and F. D. Nielsen, "Amplifiers and Lasers in PCF Configurations", Journal of Optical and Fiber Communications, vol.1 pp. 63-83, 2006.
[15] O. Ayodele, "Numerical and experimental investigation of novel materials for laser and amplifier operations," PhD thesis, University of Nottingham, 2015.
[16] T.A. Briks, J.C. Knight, and P.St. Russell, "Endlessly Single-Mode Photonic Crystal Fiber, " Opt. Lett., vol. 22**,** no**.** 13, pp. 961–963, 1997.
[17] G. Pelosi, R. Coccioli, and S. Selleri, "Microwave Guidance Structure: characterization" in Quick Finite Elements for Electromagnetic Waves, 2'nd ed. ARTECH HOUSE, pp.59-82, 2009.
[18] Z. Tang et al, "Mid-infrared photoluminescence in small-core fiber of praseodymium-ion doped selenide-based chalcogenide glass," Opt. Mater. Express vol.5, pp.870-886, 2015.
[19] E. A. Anashkina and A. V. Kim, "Numerical Simulation of Ultrashort Mid-IR Pulse Amplification in Praseodymium Doped Chalcogenide Fibers," J. Lightwave. Technol., vol. 35, no. 24, pp. 5397-5403, 2017.